



Three-dimensional architecture of a mechanoreceptor in the brown planthopper, *Nilaparvata lugens*, revealed by FIB-SEM

Jian-Sheng Guo¹ · Xin-Qiu Wang² · Dan-Ting Li² · Dan-Dan Song¹ · Chuan-Xi Zhang^{2,3} 

Received: 19 August 2019 / Accepted: 6 October 2019 / Published online: 25 November 2019
© Springer-Verlag GmbH Germany, part of Springer Nature 2019

Abstract

Trichoid sensilla are the most common mechanoreceptors in insects; depending on their distribution, they can act as either exteroceptors or proprioceptors. In this study, the internal structure of the trichoid sensillum from *Nilaparvata lugens* was studied, using focused ion beam scanning electron microscopy (FIB-SEM). We reconstructed a three-dimensional (3D) model derived from the FIB-SEM data set. The model displayed characteristic mechanosensory sensilla components, including a hair inserted in the socket, a dendrite going through the laminated cuticle, and an electron-dense tubular body at the dendrite terminal. The detailed 3D model showed the relationship between the microtubules within the tubular body and those outside of the tubular body. We also found an autocellular junction in the tormogen cell, indicating that the tormogen cell grows around the dendrite sheath to form a hollow column shape during sensilla morphogenesis.

Keywords Brown planthopper · Focused ion beam scanning electron microscopy · 3D reconstruction · Trichoid sensilla · Mechanosensory receptor

Introduction

Mechanoreceptors are specialized receptor organs that detect mechanical stimuli from a variety of external forces or self-movement, including air or water movements, air currents, the deformation of body regions, touch, and sound. In insects, the exoskeleton serves as a barrier against water, ions, and chemical movement from the environment and covers the surface of insects to maintain an appropriate internal environment; however, it can simultaneously obstruct the detection of changes in the environment (Klowden 2008). Therefore, many mechanoreceptors are located in the cuticle to detect skeletal strains,

joint movements, and external stimuli, and trichoid sensilla are among the simplest and most common mechanoreceptors (French 1988). Trichoid sensilla are distributed on nearly every part of the insect body surface and detect hair deflections caused by external and internal forces. The general organization of a trichoid sensillum has long been described as a hair inserted into a cuticular socket, under which a bipolar sensory neuron can be found (Ban et al. 2015; Thurm 1964). The distal dendrite of a sensory neuron is wrapped by dense material, and these dendrites often have modified ciliary structures, with elaborate microtubular arrangements (Keil 1997). The hair, the socket, and the neuron form a series of linked structures that are essential for mechanical coupling and transduction.

Electron microscopic (EM) studies of mechanoreceptors in insects were first performed over half a century ago (Thurm 1964). Studies examining trichoid sensilla morphology have been limited to transmission electron microscopy (TEM) images, obtained from ultrathin, resin-embedded tissues, and scanning electron microscopy (SEM). However, the imaging techniques used in the past studies have been unable to reconstruct the sensilla, and single EM sections of the sensilla do not provide a detailed view to determine how the structures are spatially arranged. Focused ion beam scanning electron microscopy (FIB-SEM) data with high z-resolution (5 nm in this study) can precisely determine the three-dimensional (3D) ultrastructure of the sensilla.

Jian-Sheng Guo and Xin-Qiu Wang contributed equally to this work.

Electronic supplementary material The online version of this article (<https://doi.org/10.1007/s00441-019-03122-7>) contains supplementary material, which is available to authorized users.

✉ Chuan-Xi Zhang
chxzhang@zju.edu.cn

¹ School of Medicine, Zhejiang University, Hangzhou 310058, China

² Institute of Insect Science, Zhejiang University, Hangzhou 310058, China

³ Institute of Plant Virology, Ningbo University, Ningbo 315211, China

Brown planthoppers (BPHs), *Nilaparvata lugens* (Hemiptera: Delphacidae), walk and jump on rice plants, and various sensilla in the cuticle enable BPHs to respond quickly to the changing environment, playing important roles in feeding, migration, and reproduction. Mechanosensory sensilla in the antennae and mouthparts of *N. lugens* have been studied morphologically (Aljunid and Anderson 1983; Brozek and Bourgoin 2013; Fu et al. 2012). However, the mechanosensory sensilla found in other parts of this species have not been studied.

In this study, we determined the 3D structure of mechanosensory trichoid sensilla using FIB-SEM and developed a 3D structural model of trichoid sensilla found on the sternite of BPHs. The cuticular components were segmented and presented separately in the model, allowing their spatial relationship to be clearly observed and providing an understanding of coupling mechanism required for mechanosensory function. The detailed 3D model also showed the relationship between the microtubules within the tubular body and those found in the remainder of the dendrite. We tracked the tormogen cell and discovered an autocellular junction in the tormogen cell. These updated structural data provided insights into trichoid sensilla structure and morphogenesis.

Materials and methods

Insects

The BPHs used in this study were originally collected in Hangzhou (30° 16' N, 12° 11' E), China. The BPHs were reared at 26 ± 0.5 °C, on rice seedlings, under a 16:8 h (light:dark) photoperiod.

Samples and preparation

Sternites were collected from fifth instar nymphs, 48 h after molting, using tweezers and a razor blade. The samples were quickly fixed for 24 h in 0.1 M sodium cacodylate (Sigma, CAS: 6131-99-3) buffer containing 2% paraformaldehyde (Sigma, CAS: 30525-89-4), 2.5% glutaraldehyde (TED PELLA, Lot No.: 2171002), and 0.003% CaCl₂ (Sigma, C-2661-500G). The tissue blocks were then washed in sodium cacodylate buffer (0.1 M) and treated with a solution containing equal volumes of 2% OsO₄ (TED PELLA, Lot No: 4008-160501) and 3% potassium ferrocyanide (Sigma, CAS: 14459-95-1), in 0.3 M sodium cacodylate, containing 4 mM CaCl₂, for 1 h on ice. After rinsing with double-distilled water (ddH₂O), the samples were incubated in 1% thiocarbohydrazide (Sigma, CAS: 2231-57-4) (in water) for 20 min at room temperature. Then, the samples were rinsed in ddH₂O and treated with 2% aqueous OsO₄ for 30 min at room temperature. The tissue blocks were washed in ddH₂O and

immersed overnight, at 4 °C, in 1% aqueous uranyl acetate. After washing with ddH₂O, the samples were incubated in 0.66% lead nitrate (Sigma, CAS: 10099-74-8) diluted in 0.03 M L-aspartic acid (Sigma, CAS: 56-84-8) (pH 5.5) for 30 min at 60 °C, and then dehydrated and flat-embedded in EPON 812 resin (EMS, cat. no: 14900) for 48 h at 60 °C.

FIB-SEM data collection

Resin blocks were carefully trimmed, using a Leica EM trimmer, until the surface of the black tissue in the block could be observed. To obtain the area of interest, we used a scanning electron microscope (Thermo Fisher, Teneo VS), with one ultramicrotome in its specimen chamber, which allowed the resin blocks to be trimmed and the electron microscopic image of the sample to be acquired synchronously. After identifying the area of interest, imaging was performed using dual-beam SEM (Thermo Fisher, FIB Helios G3 UC). The data were collected in serial surface view mode, with a slice thickness of 5 nm, at 30 keV, and 0.79 nA. Each serial face was then imaged with an acceleration voltage of 2 kV and a current of 0.2 nA, in backscatter mode (BSE), with an in-column backscatter electron detector (BSD). The image storage resolution was set to 3072 × 2048 pixels, with a dwell time of 15 μs per pixel, and a lateral resolution of 4.25 nm per pixel.

Image processing and segmentation

The image stack was aligned and cropped, using IMOD (Boulder Laboratory) and Amira 6.5 (Thermo Fisher). The cuticle and sensilla were segmented and labeled manually, using Amira 6.5. Finally, surface-generation tools were used to compute the surfaces, using Amira 6.5. The resulting surface file was simplified to 10% of the original value and saved as a Wavefront file (.obj). The resulting file was reassembled, colored, and rendered into images in Cinema 4D (Maxon Computer, Germany). An interactive 3D Portable Document Format (PDF) file was created, as described by de Bakker et al. (de Bakker et al. 2016)

Conventional SEM

Adult BPH were fixed in 2.5% glutaraldehyde in phosphate-buffered saline (PBS) buffer (pH 7.4) and post-fixed in 1% OsO₄. Dehydration was carried out in an ethanol dilution series (30%, 50%, 70%, and 90%, followed by 3 × 100%). After critical drying with an automated critical point dryer (Leica, EM CPD300), the samples were mounted on double-sided carbon tape on holders and plasma-coated with 8 nm gold, and then investigated using a conventional scanning electron microscope (Thermo Fisher, Helios). SEM images were colored in Adobe Photoshop.

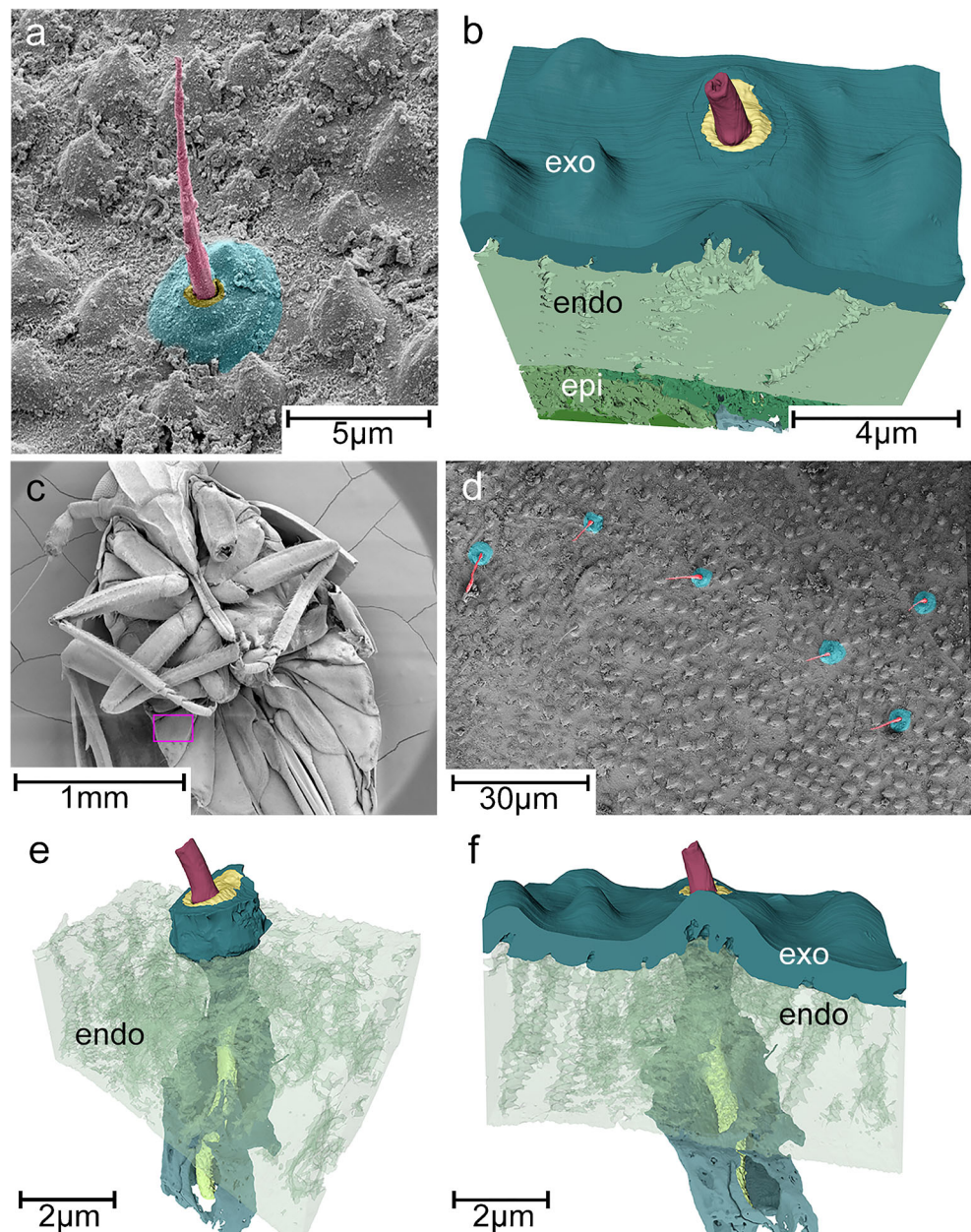
Results

The external structure of trichoid sensilla in *N. lugens*

Two trichoid sensilla were studied using FIB-SEM and recreated as 3D structural models. We chose one as an example and focused on the common features they shared. The hair was too long to remain intact during sample preparation (Fig. 1a); therefore, we were only able to reconstruct the hair base, instead of the full length (Fig. 1b). The cuticular components and peripheral cells were clearly tracked through a set of images, with nearly 600 serial cross-sections (Online Resource 3).

Conventional SEM was utilized to investigate the external structures of approximately 50 trichoid sensilla on the sternite (Fig. 1c). The resulting conventional SEM images were in accordance with the external morphology of the reconstructed 3D model (Fig. 1a, b). On the sternite of *N. lugens*, randomly distributed trichoid sensilla appeared as sharp-tipped hairs inserted into elliptical, bulging, oval cuticular sockets, and the hairs all tilted to lateral and posterior positions (Fig. 1d). Based on the 50 sensilla, we measured, the long axis of the socket was $4.8 \pm 0.5 \mu\text{m}$ (mean \pm SD), and the short axis of the socket was $3.8 \pm 0.5 \mu\text{m}$ (mean \pm SD). The length of the hair was $11.8 \pm 1.6 \mu\text{m}$ (mean \pm SD), and the diameter of the hair was $895 \pm 163 \text{ nm}$ (mean \pm SD).

Fig. 1 External morphology of the trichoid sensillum. **a** SEM image of a trichoid sensillum. Red represents the hair; yellow represents the joint membrane; cyan represents the cuticular socket. **b** Reconstructed model of the sensillum. exo, exocuticle; endo, endocuticle; epi, epidermis. **c** Ventral view of the BPH by SEM. The sensilla we studied were in the boxed area. **d** Sensilla from the boxed area in Fig. 1c, viewed by SEM. The hairs all tilted to lateral and posterior positions. **e** Reconstructed model of the sensillum, with the exocuticle removed and the endocuticle transparent. **f** Reconstructed model of the sensilla, with the endocuticle transparent



Three-dimensional structural model of the trichoid sensilla

The inner part of the sensilla went through the exocuticle and the endocuticle (Fig. 1e, f), and FIB-SEM images showed the internal structure (Fig. 2a, b). In these serial-section images,

the cuticular socket appeared to be part of the exocuticle and could be observed as a bump in the cuticle. The hollow hair base connected to the cuticular socket via the joint membrane. In addition to the direct connection between the joint membrane and the socket, the hair and the socket were also connected via a few suspension fibers, which are believed to

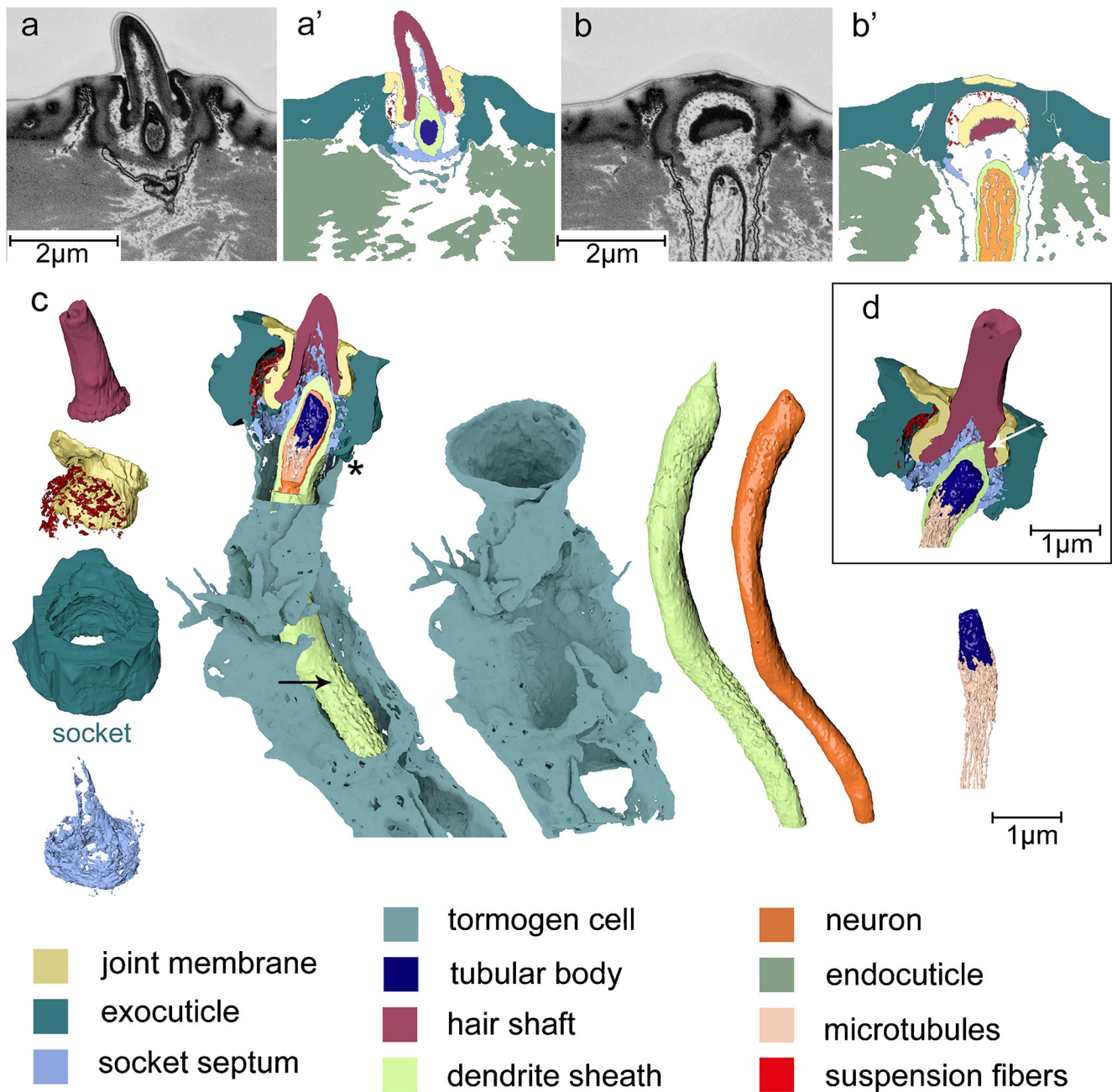


Fig. 2 Sensillum organization. (a, a', b, and b') Two representative side-on views of the sensillum, taken from the FIB-SEM dataset, are shown in a and b. The structures were segmented and presented in a' and b'. (c) Model of the separated components, with an assembled sensillum model on the right. In the assembled sensillum model, half of the socket, joint membrane, hair base, suspension fibers, socket septum, tormogen cell, dendrite sheath, and neuron were removed to clearly present the spatial

relationships among the components. The arrow indicates protrusions on the surface of the dendrite sheath. The asterisk indicates the tight contact between the apical surface of the tormogen cell and the socket. This model was produced by segmenting components in every slice from the FIB-SEM dataset, as shown in Fig. 1a, a', b, and b'. (d) A cross-section of the distal end of the reconstructed sensillum model. The arrow indicates the touching point of the dendrite sheath and the hair base

restrict the extent of the hair base movement (Di Giulio et al. 2012; Guthrie 1966). Inside the hollow hair base, the distal end of the dendrite was found, tightly wrapped by the dendrite sheath and separated from the endocuticle by the tormogen cell. A cytoplasmic reticulum, named the socket septum, connected the socket and the dendrite sheath. The sensilla structure was better visualized in the 3D model (Figs. 2c, 3, and 4) and in the interactive 3D PDF file (Online Resource 1).

The joint membrane formed a hollow cylinder, with the lower end connected to the hair base and the upper end connected to the cuticular socket. The socket septum connected the socket and the dendrite sheath (Fig. 2c, d), and part of the socket septum wrapped the dendrite sheath. As a result, it appeared in the shape of a pointy hat in the 3D view. The dendrite sheath was approximately 50 nm thick, with some protrusions on the surface (Fig. 2c). It tightly enclosed the dendrite, without any gaps, with its pointy distal end touching one side of the hair base (Fig. 2d).

The soma of the sensory neuron was not shown in the model because it was deep in the epidermis and did not appear in any images. The cross-section of the dendrite was nearly round, with a diameter of 600 nm. In the distal end of the dendrite, a cylindrical tubular body appeared as an electron-dense material with a length of 850 nm and a diameter of 500 nm (Online Resource 1, showing the 3D structure of the tubular body).

Autocellular junction of the tormogen cell

The tormogen cell formed an envelope around the dendrite sheath (Fig. 2c), leaving a sensillum lymph space (Moran et al. 1976) between the dendrite sheath and the tormogen cell (Fig. 3e–g). Its apical surface was tightly connected to the socket (Fig. 2c). The tormogen cell shaped like a hollow column, and we found two types of junctions within it. At the distal end of the tormogen cell, looking from the distal end towards the proximal end, the tormogen cell formed a circle around the dendrite sheath. At the junction where the two sides of the tormogen cell met, one side formed a groove and the other side was inserted into this groove (Fig. 3b, e). The junction was tight, with the plasma membranes appearing to touch (Fig. 3e). The groove could be found from the top of the tormogen cell to 500 nm below the top of the tormogen cell (Fig. 3c), and the membranes remained tightly connected (Fig. 3f). Below this section, the groove disappeared, the two ends of the cell overlapped, and the plasma membranes remained tightly connected (Fig. 3d, g). When we looked further down, the overlapping structure continued until 3 μm under the distal end, when the two ends of the cell separated (Fig. 3a).

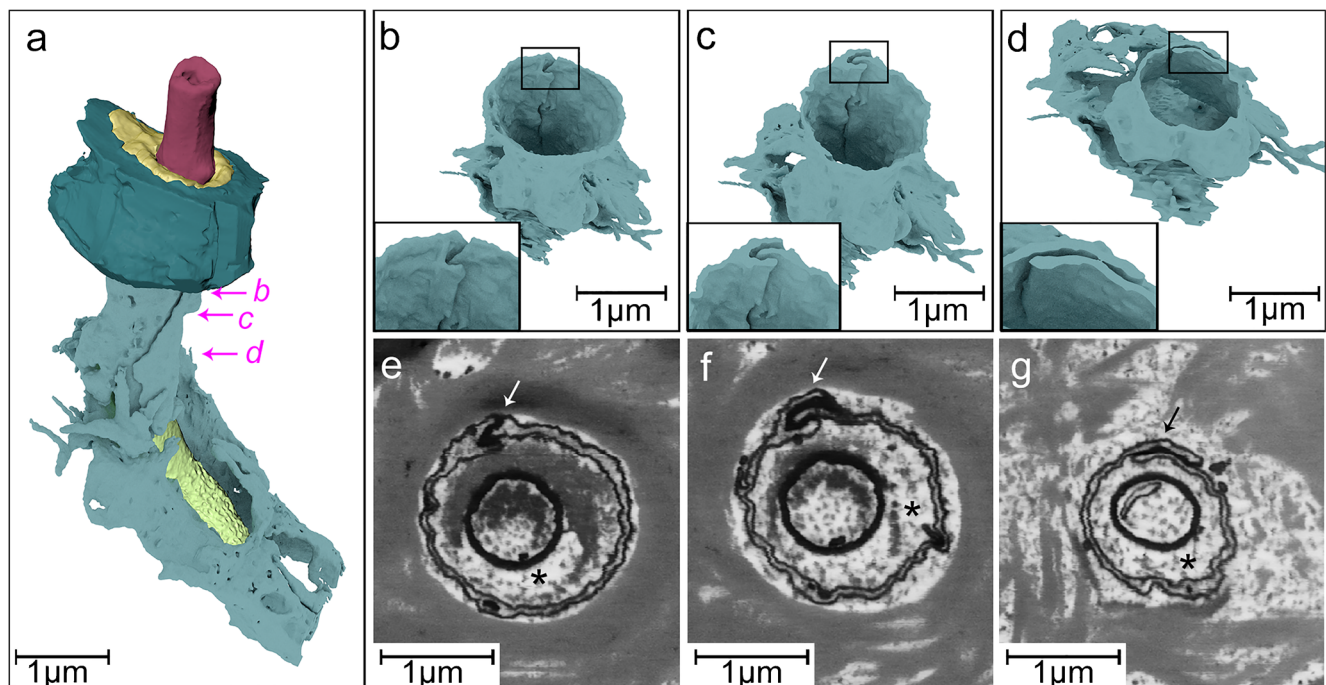


Fig. 3 Trichoid sensilla structure and the junction in the tormogen cell. **a** Overview of the structural model. The structural components are in different colors, following the color key presented in Fig. 2. **b–d** End-on cross-section views that correspond with the locations marked in Fig. 3a by magenta arrows, showing progressive changes in the junction from the distal end to the middle of the dendrite. **e, f** Cross-sections of the

sensillum at 50 nm, 500 nm, and 1,500 nm from the distal end of the tormogen cell. The FIB-SEM images were sagittal sections, and the cross-sections were made in Amira by aligning the FIB-SEM images. The outer circle is the tormogen cell, and the inner circle is the dendrite sheath, which wrapped the neuron tightly. The arrows indicate the junctions, and the asterisks indicate sensillum lymph spaces

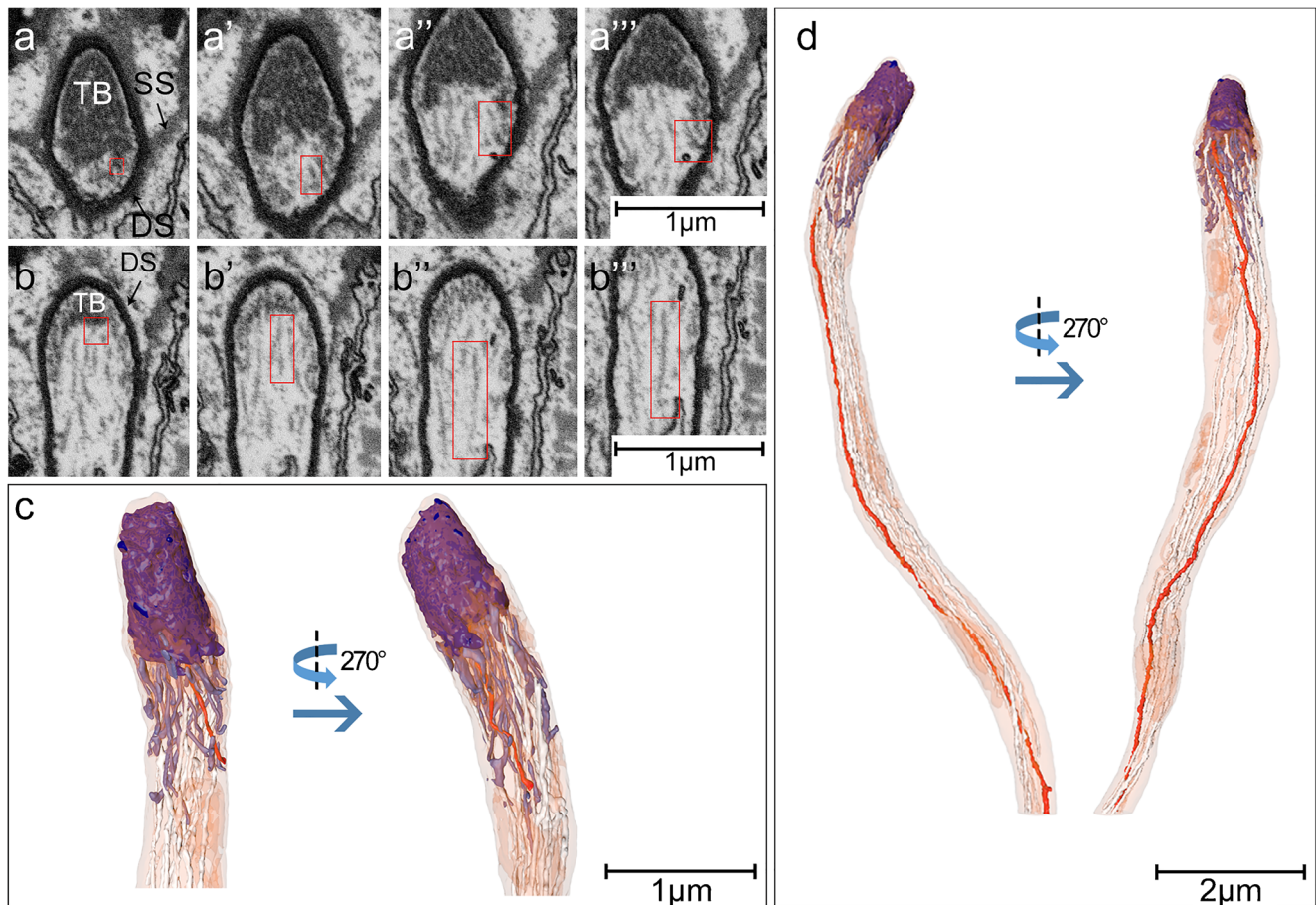


Fig. 4 Microtubules in the tubular body and the remainder of the dendrite. (a, a', a'', and a''') Side-on views of sequential, cross-sectional FIB-SEM images of a representative microtubule, from the tubular body to the neuron cell membrane (left to right). The boxed microtubule corresponds to the red microtubule in c. DS, dendrite sheath; TB, tubular body. (b, b', b'', and b''') Side-on views of sequential, cross-sectional FIB-SEM images of a representative microtubule, from the tubular body to the middle of the dendrite (left to right). The boxed microtubule ran parallel

to the longitudinal axis of the dendrite and corresponds with the red microtubule in Fig. 4d. SS, socket septum. (c) Distal end of the dendrite. In the transparent dendrite, microtubules from the cell membrane (dark) and from the proximal end of the dendrite (light) join together to form the tubular body (purple). The red microtubule is one of the microtubules from the cell membrane. (d) Distal end of the dendrite. The microtubules, tubular body, and dendrite follow the color key in Fig. 4c. The red microtubule is one of the microtubules that run parallel to the dendrite

Microtubules in the tubular body and in the remainder of the dendrite

The tubular body was formed by tightly packed bundles of microtubules. The tubular body was approximately 50 nm in diameter. The microtubules become more dispersed in the remainder of the dendrite (Fig. 2c), and fewer than those observed in the tubular body. Some microtubules passed through the dendrite, but the number was not constant because microtubules can break when stretching distally.

The microtubules in the dendrite have been described as regularly organized within the tubular body and freely arranged throughout the remainder of the distal dendrite (French 1988). The numbers of microtubules that form the

tubular body can vary between species and locations, from 30 in the tsetse fly (Rice et al. 1973), 100–150 in the haltere sensilla of *Drosophila* (Chevalier 1969), to approximately 1,000 in the cockroach (Keil 1997). In this study, 42 microtubules were found to form the tubular body, while the number of microtubules found in the proximal end of the dendrite was much lower. To analyze how microtubule numbers increased from the proximal part of the dendrite to the tubular body, we tracked every microtubule through the 600 images. Among the 42 microtubules that formed the tubular body, 11 microtubules originated from the proximal part of the dendrite (Fig. 4b, b', b'', b''', and d), and 31 microtubules were approximately 1 μm in length, with their proximal end connecting to the plasma membrane (Fig. 4a, a', a'', a''', and c).

Discussion

Possible coupling mechanism

Gaffal et al. (1975), French (1988), and Tao and Yu (2012) have reviewed the functional structures of cuticular mechanosensory sensilla. The sensillum we described here has a similar structure to those of known mechanosensory trichoid sensilla, and they all share the following characteristic features: the cuticular hair, the cuticular socket, and the tubular body. These components form a series of linked structures that produce a generator potential in the dendrite that can respond to deflection of the hair. Studies examining the thorax trichoid sensilla in the cabbage moth, *Barathra brassicae*, and the tactile hairs in the locust, *Schistocerca gregaria*, have demonstrated that trichoid sensilla have directional sensitivity (Kalogianni 1995; Matheson 2012; Newland 1991; Schroeder et al. 2018; Tautz 1978). They proposed that the joint membrane was flexible to permit hair deflection and that the neuron generally produced the strongest action potential if the hair was bent in the direction where the tip of the dendrite was inserted. Matsumoto suggested that bending the hair on the ventral surface of the blowfly ventrally caused the hair base to compress the tubular body, bending the microtubules in the tubular body (Matsumoto and Farley 1978).

The structural properties of the trichoid sensillum that we reconstructed can partly elucidate its coupling function. In this case, the distal end of the dendrite sheath was attached to the right side of the hair base, and lower part of the dendrite sheath connected the socket via the socket septum to restrict the movement of the dendrite sheath (Fig. 2d). Rightward movements of the hair will result in leftward movements of the hair base, and the dendrite sheath can easily be pressed by the hair base at the connecting site (arrow in Fig. 2d). The socket septum immobilizes the dendrite sheath, preventing the dendrite from moving when pressed by the hair base, causing the tubular body to become pinched by the dendrite sheath following hair movement and creating the generator potential. However, when hair is bent in the opposite direction, the right side of the hair base will move rightwards, the hair base will leave the dendrite sheath, and the tubular body in the dendrite sheath will remain uninfluenced, creating no generator potential.

The tubular body is believed to be the mechanosensory transduction site, where the mechanical stimuli are transduced into electrical signals (Bechstet et al. 2010; Liang et al. 2011). The microtubules in the tubular body have been reported to maintain some connections with the cell membrane via membrane-microtubule connectors (MMCs), which contain no mechanoreceptor potential C (NompC) components (Sun et al. 2019). This connection is believed to play an important role in mechanical transduction because NompC belongs to a transient receptor potential channel family of ion channels (Liang et al. 2013). The MMCs were not reconstructed in

our study because the resolution was not sufficiently high to clearly observe MMCs. In this study, we found that the tubular body can also connect with the plasma membrane, via short microtubules. Microtubules in a neuron are used to transport substances to different parts of the cell, whereas short mobile microtubules in the dendrite might convey signaling molecules as they transit within the neuron (Dent and Baas 2014). We did not find any short microtubules transporting organelles in the FIB-SEM data; therefore, whether they act as information carriers remains unknown.

The autocellular junction implied the morphogenesis of the tormogen cell

Previous studies have demonstrated that tormogen cells and trichogen cells form a tight seal between the sensillum lymph space and the subcuticular spaces (Küppers and Thurm 1979). The tight contact between the apical membrane of the tormogen cell and the cuticle of the hair base in the olfactory sensilla of *Antheraea Polyphemus* was believed to be the structural basis for the electrical isolation that occurs between the sensillum lymph space and subcuticular spaces (Keil 1984). The high potassium concentration in the sensillum lymph space has been shown to create transepithelial potential differences in several insect species (Küppers 1974). The tight contact between the apical membrane of the tormogen cell and the socket, and the autocellular junction made tormogen cell a barrier between the sensillum lymph space and the subcuticular space.

The tight autocellular junction may be formed by the wrapping of the tormogen cell. The most accepted understanding of mechanosensory trichoid sensilla morphogenesis in *Drosophila melanogaster* is that the four cells found in each trichoid sensillum, namely the neuron, the thecogen cell, the trichogen cell, and the tormogen cell, all derive from a sensillum mother cell. The tormogen cell grows around the dendrite sheath and secretes the socket and joint membrane at the hair base; then, it retracts and only the peripheral part attached to the exocuticle remains. Finally, the tormogen cell forms a hollow column shape, and the sensillum lymph space appears (Hartenstein and Posakony 1989). The wrapping of the tormogen cell produces a visible autocellular junction where the two ends of the tormogen cell meet. Although these junctions are instrumental for demonstrating that the tormogen cell grows around the dendrite sheath to form the hollow column shape during sensilla morphogenesis, their structure has not been described in previous studies. The junction is difficult to identify in conventional TEM images (see an example of the TEM image in Fig. S1, Online Resource 2) because the ultrathin samples slices used for TEM observations may not contain the junction. In the FIB-SEM data set, every part of the tormogen cell was observed in the serial-sectioned EM images; therefore, the tormogen cell could be tracked over hundreds of sections.

Conclusion

The spatial relationships among the cuticular components and their relative positions within the cuticle were revealed by FIB-SEM and then reconstructed into a 3D model that presented the general structural features of mechanosensory trichoid sensilla. The morphology of tormogen cells and the microtubules in the dendrite can be difficult to study using conventional TEM because they are irregularly shaped, and only parts of them are visible in a single cross-section (see an example of the TEM image in Fig S1 in Online Resource 2). In contrast, FIB-SEM represents a powerful technique for studying the 3D structure of the sensilla. We can study the progressive changes of the tormogen cell across hundreds of images. However, this technique is most useful when studying small samples (for example, $40 \times 40 \times 40 \mu\text{m}$); therefore, we were unable to examine the inner part of the dendrite or the entire tormogen cell. The 3D structure allowed us to study details of the sensilla that have not been previously revealed during past EM studies.

Funding information This work was supported by the National Natural Science Foundation of China, grants 31630057 and 31471765.

Compliance with ethical standards

Conflict of interest The authors declare that they have no conflict of interest.

Ethical approval All applicable international, national, and/or institutional guidelines for the care and use of animals were followed.

Informed consent Not applicable.

References

- Aljumid SF, Anderson M (1983) Ultrastructure of sensilla on the antennal pedicel of the brown planthopper *Nilaparvata-lugens* Stal (Insecta, Homoptera) - I. Plaque organs and trichoid sensilla. *Cell Tissue Res* 228:313–322
- Ban L-P, Sun Y-P, Wang Y, Tu X-B, Zhang S-G, Zhang Y-T, Wu Y-S, Zhang Z-H (2015) Ultrastructure of antennal sensilla of the peach aphid *Myzus persicae* sulzer, 1776. *J Morphol* 276:219–227. <https://doi.org/10.1002/jmor.20335>
- Bechstet S, Albert JT, Kreil DP, Muller-Reichert T, Gopfert MC, Howard J (2010) A doublecortin containing microtubule-associated protein is implicated in mechanotransduction in *Drosophila* sensory cilia. *Nat Commun* 1:1–11. <https://doi.org/10.1038/ncomms1007>
- Brozek J, Bourgoin T (2013) Morphology and distribution of the external labial sensilla in Fulgoromorpha (Insecta: Hemiptera). *Zoomorphology* 132:33–65. <https://doi.org/10.1007/s00435-012-0174-z>
- Chevalier RL (1969) The fine structure of campaniform sensilla on the halteres of *Drosophila melanogaster*. *J Morphol* 128:443–463
- de Bakker BS, de Jong KH, Hagoort J, de Bree K, Besselink CT, de Kanter FE, Veldhuis T, Bais B, Schildmeijer R, Ruijter JM, Oostra RJ, Christoffels VM, Moorman AFM (2016) An interactive three-dimensional digital atlas and quantitative database of human development. *Science* 354:1019 aag0053+–
- Dent EW, Baas PW (2014) Microtubules in neurons as information carriers. *J Neurochem* 129:235–239. <https://doi.org/10.1111/jnc.12621>
- Di Giulio A, Maurizi E, Stacconi MV, Romani R (2012) Functional structure of antennal sensilla in the myrmecophilous beetle *Paussus favieri* (Coleoptera, Carabidae, Paussini). *Micron* 43:705–719. <https://doi.org/10.1016/j.micron.2011.10.013>
- French AS (1988) Transduction mechanisms of mechanosensilla. *Annu Rev Entomol* 33:39–58
- Fu BX, Bellis G-A, Hong J, Wang J-R, Wu Q, Tang Q-Y, Cheng J-A, Zhu Z-R (2012) Morphology, distribution, and abundance of antennal sensilla of male and female macropterous and brachypterous small brown planthopper, *Laodelphax striatellus* (Fallen) (Hemiptera: Delphacidae). *Microsc Res Tech* 75:1492–1512. <https://doi.org/10.1002/jemt.22093>
- Gaffal KP, Tichy H, Theiß J, Seelinger G (1975) Structural polarities in mechanosensitive sensilla and their influence on stimulus transmission (Arthropoda). *Zoomorphologie* 82:79–103. <https://doi.org/10.1007/bf00993585>
- Guthrie DM (1966) The function and fine structure of the cephalic airflow receptor in *Schistocerca gregaria*. *J Cell Sci* 1:463–470
- Hartenstein V, Posakony JW (1989) Development of adult sensilla on the wing and notum of *Drosophila melanogaster*. *Development* 107:389–405
- Kalogianni E (1995) Physiological properties of wind-sensitive and tactile trichoid sensilla on the ovipositor and their role during oviposition in the locust. *J Exp Biol* 198:1359–1369
- Keil TA (1984) Very tight contact of tormogen cell membrane and sensillum cuticle: Ultrastructural basis for high electrical resistance between receptorlymph and subcuticular spaces in silkworm olfactory hairs. *Tissue Cell* 16:131–135
- Keil TA (1997) Functional morphology of insect mechanoreceptors. *Microsc Res Tech* 39:506–531
- Klowden MJ (2008) *Physiological Systems in Insects*. Academic Press, Cambridge
- Küppers J (1974) Measurements on the ionic milieu of the receptor terminal in mechanoreceptive sensilla of insects. In: *Symposium Mechanoreception: Abhandlungen der Rheinisch-Westfälischen Akademie der Wissenschaften*. VS Verlag für Sozialwissenschaften, Wiesbaden, pp 387–394.
- Küppers J, Thurm U (1979) Active ion transport by a sensory epithelium. *J Comp Physiol* 134:131–136. <https://doi.org/10.1007/bf00610471>
- Liang X, Madrid J, Saleh HS, Howard J (2011) NOMPC, a member of the TRP channel family, localizes to the tubular body and distal cilium of *Drosophila* campaniform and chordotonal receptor cells. *Cytoskeleton* 68:1–7. <https://doi.org/10.1002/cm.20493>
- Liang X, Madrid J, Gärtner R, Verbavatz J, Schiklenk C, Wilsch-Braeuning M, Bogdanova AI, Stenger F, Voigt A, Howard J (2013) A NOMPC-dependent membrane-microtubule connector is a candidate for the gating spring in fly mechanoreceptors. *Curr Biol* 23:755–763
- Matheson T (2012) *The insects: Structure and function*, fifth edn. Cambridge University Press, Cambridge
- Matsumoto DE, Farley RG (1978) Comparison of the ultrastructure of stimulated and unstimulated mechanoreceptors in the taste hairs of the blowfly *Phaenicia serricata*. *Tissue Cell* 10:63–76
- Moran DT, Rowley JC, Zill SN, Varela FG (1976) The mechanism of sensory transduction in a mechanoreceptor. Functional stages in campaniform sensilla during the molting cycle. *J Cell Biol* 71:832–847. <https://doi.org/10.1083/jcb.71.3.832>
- Newland PL (1991) Physiological-properties of afferents from tactile hairs on the hindlegs of the locust. *J Exp Biol* 155:487–503

- Rice MJ, Galun R, Margalit J (1973) Mouthpart sensilla of the tsetse fly and their function: III: Labrocibarial sensilla. *Ann Trop Med Parasitol* 67:109–116
- Schroeder TBH, Houghtaling J, Wilts BD, Mayer M (2018) It's not a bug, it's a feature: functional materials in insects. *Adv Mater*. <https://doi.org/10.1002/adma.201705322>
- Sun L, Gao Y, He J, Cui L, Meissner J, Verbavatz JM, Li B, Feng X, Liang X (2019) Ultrastructural organization of NompC in the mechanoreceptive organelle of *Drosophila* campaniform mechanoreceptors. *Proc Natl Acad Sci* 116:7343–7352
- Tao J, Yu B (2012) Hair flow sensors: From bio-inspiration to biomimicking - a review. *Smart Mater Struct*. <https://doi.org/10.1088/0964-1726/21/11/113001>
- Tautz J (1978) Reception of medium vibration by thoracic hairs of caterpillars *Ofbarathra brassicae* L. (Lepidoptera, Noctuidae). *J Comp Physiol* 125:67–77. <https://doi.org/10.1007/bf00656832>
- Thurm U (1964) Mechanoreceptors in the cuticle of the honey bee: fine structure and stimulus mechanism. *Science* 145:1063–1065. <https://doi.org/10.1126/science.145.3636.1063>

Publisher's note Springer Nature remains neutral with regard to jurisdictional claims in published maps and institutional affiliations.